Improvement in activity and alkali resistance of a novel V-Ce$(SO_4)_2$/Ti catalyst for selective catalytic reduction of NO with NH_3

Wenshuo Hu [a, b], Yuhong Zhang [a], Shaojun Liu [b, c], Chenghang Zheng [a], Xiang Gao [a,*], Isabella Nova [b], Enrico Tronconi [b,**]

[a] *State Key Laboratory of Clean Energy Utilization, Zhejiang University, 38 Zheda Road, Hangzhou, Zhejiang PRC, 310027, China*

[b] *Laboratory of Catalysis and Catalytic Processes, Dipartimento di Energia, Politecnico di Milano, Via La Masa 34, Milano, 20156, Italy*

[c] *School of Energy and Power Engineering, Jiangsu University of Science and Technology, 2 Mengxi Road, Zhenjiang, Jiangsu PRC, 212003, China*

* Corresponding author. Tel.: +86 571 87951335.

** Corresponding author. Tel.: +39 02 23993264

E-mail address: xgao1@zju.edu.cn (X. Gao), enrico.tronconi@polimi.it (E. Tronconi).

Abstract

A series of V-$Ce(SO_4)_2$/Ti catalysts for selective catalytic reduction (SCR) of NO with ammonia are prepared by impregnation method. Low temperature SCR activity and alkali resistance of the optimal V-0.5$Ce(SO_4)_2$/Ti sample are found to be better than on the commercial V-W/Ti catalyst. Also, V-0.5$Ce(SO_4)_2$/Ti shows an excellent durability in the presence of SO_2 and H_2O, indicating to have prospects for the industrial application.

Based on catalysts characterization and in-situ DRIFTS studies, a higher proportion of surface active oxygen generated by the introduction of Ce and a much faster H_2 reduction point out the improved redox properties of V-0.5$Ce(SO_4)_2$/Ti, which results in a stronger NO oxidative activation and is confirmed by a more abundant formation of surface NO^+ and NO_3^- species. When exposed to SCR conditions where both NH_3 and NO are present, this enhanced NO activation can produce more reactive nitrite and/or NO^+ intermediates which then readily react with adsorbed NH_3 and decompose to N_2 and H_2O, accounting for the improved SCR activity of V-0.5$Ce(SO_4)_2$/Ti at low temperatures.

The addition of $Ce(SO_4)_2$ also provides abundant reactive acid sites and adsorbed NH_3 species thus increase. Even after Na poisoning, adequate surface acidity and redox properties still remain. Furthermore, relatively higher contents of V-OH are preserved owing to the interaction between Na and O=S=O, acting as a protection for the active sites. These promotional effects contribute to the better alkali resistance of V-0.5$Ce(SO_4)_2$/Ti. Therefore, all the results suggest that V-0.5$Ce(SO_4)_2$/Ti is a promising candidate as a catalyst for NH_3-SCR in coal-fired power plants, especially under high Na-content conditions.

Key words: Vanadium; $Ce(SO_4)_2$; redox properties; acidity; alkali resistance

1 Introduction

Selective catalytic reduction (SCR) with NH_3/urea is currently one of the most effective methods for the abatement of NOx emissions from stationary sources and diesel vehicles [1-3]. V_2O_5-WO_3/TiO_2 and V_2O_5-MoO_3/TiO_2 catalysts were commercialized for stationary applications three decades ago. However, these conventional catalysts are effective only within a narrow temperature range of 300-400 ˚C and can be easily affected by poisonous elements in the flue gas. Alkali metals, especially K and Na, are reported to be a major concern [4, 5]. Therefore, many efforts have been made to broaden the active temperature window of SCR catalysts and increase their resistance to alkali metals.

Some metal oxides, such as MnOx, CuO, Fe_2O_3 and CeO_2, have been widely investigated and found to be active in SCR reactions [6]. More recently, cerium based oxides attracted much attention due to their high oxygen storage capacity and excellent redox properties. A series of CeO_2 containing catalysts, including VOx/CeO_2, MnOx-CeO_2, CeO_2-Nb_2O_5, CeO_2-WO_3 and CeO_2-WO_3/TiO_2, have shown excellent SCR activities at low temperature (low-T) [6-9]. However, CeO_2 based catalysts are proven to be sensitive to SO_2 poisoning, which has become an essential factor to limit their potential application since flue gas always contains large amounts of SO_2 [10]. As for the deactivation of alkali metals, various studies have revealed that both surface acidity and redox properties of SCR catalysts decrease seriously after alkali-poisoning [5, 11]. Even though some of these CeO_2 containing catalysts exhibit a good alkali resistance, their sensitivity to SO_2 is an additional restriction, as mentioned above. Therefore, enhancing the low-T activity and alkali resistance of V-based catalysts seems more feasible in industrial applications.

It is known that surface sulfates (SO_4^{2-}) can provide strong acid sites and thus improve V-based

catalysts surface acidities [12, 13]. Addition of CeO_2 into V/Ti and V-W/Ti is also reported to promote their SCR activities by enhancing the redox properties [14, 15]. It thereby seems reasonable that the simultaneous addition of Ce and SO_4^{2-} would enhance both the redox properties and the surface acidities, and has therefore potential to improve the low-T activity and alkali-resistance of V-based catalysts.

In the present work, a series of V-Ce$(SO_4)_2$/Ti catalysts were prepared to study the promotional effect of the co-addition of Ce and SO_4^{2-}. SCR performance and alkali resistance were systematically analyzed with activity and characterization experiments in comparison with commercial V-W/Ti catalysts. Besides, the effects of SO_2 and H_2O were also investigated to evaluate the feasibility of the novel V-Ce$(SO_4)_2$/Ti catalysts for industrial implementation. Finally, based on these experimental results, a mechanism is proposed to explain the observed promoting effects.

2 Experimental

2.1 Catalysts preparation

The V-Ce$(SO_4)_2$/Ti and V/Ti catalysts in this work were prepared by the impregnation method. Firstly, proper amount of Ce$(SO_4)_2$ solution were used to impregnate the TiO_2 support (P25 from Degussa, 85% anatase and 15% rutile, S_{BET}=55 m^2/g) [16], conditioned at room temperature for 12 h and dried at 110 ˚C for 6 h. The mixture were then calcined at 500 ˚C in air for 5 h. Afterwards, ammonium metavanadate (NH_4VO_3) dissolved in oxalic acid solution was used as V_2O_5 precursors and impregnated the Ce$(SO_4)_2$/Ti powders with V loading of 0.6 wt% (specific contents are measured and listed in Table S1 in the Support Information), which is a common content in commercial catalysts [2, 17]. For the V/Ti samples, TiO_2 support was directly impregnated by the

above NH_4VO_3 solution with the same V loading. Then the same conditioning, drying and calcination procedures were performed subsequently, and the catalysts were labelled as V-x$Ce(SO_4)_2$/Ti (x is the mole ratio of $Ce(SO_4)_2$/V) and V/Ti, respectively. Besides, a typical commercial V-W/Ti catalyst with similar V content (see Table S1 in the Support Information) from a power plant in China, which was originally supplied as a honeycomb monolith, has also been studied for comparison.

In this work, sodium (Na) was chosen as the representative of alkali metals, since Na is widespread in the stack gases of stationary sources, especially those of the coal-fired power plants [5, 11]. The same impregnation method was applied to dope 0.5 wt% of Na (using $NaHCO_3$ as the precursor) on the commercial and V-$Ce(SO_4)_2$/Ti catalysts, labelled as V-W-Na/Ti and V-$Ce(SO_4)_2$-Na/Ti, respectively. All the catalysts were crushed and sieved within 40-60 meshes for activity measurement.

2.2 SCR activity test

SCR activity tests were carried out in a fixed-bed quartz reactor containing 200 mg of catalysts and operated under atmospheric pressure in the range of 150-450 ˚C. The feed gas contained 800 ppm of NO, 800 ppm of NH_3, 5 vol.% O_2, 500 ppm of SO_2 (when used), 5 vol.% H_2O (when used) and N_2 as the balanced gas. The total flow rate of the feed gas was 500 ml/min, corresponding to a gas hourly space velocity (GHSV) of 150,000 ml/(g·h). Concentrations of NO, NO_2, N_2O and NH_3 were continually measured by an FT-IR spectrometer (Gasmet DX 4000 FT-IR). The SCR activity (NO conversion) and N_2 selectivity are calculated as follows [8]:

$$\text{NO conversion} = \frac{[NO]_{in}-[NO]_{out}}{[NO]_{in}} \times 100\%$$

$$\text{N}_2\text{ selectivity} = 1 - \frac{2[N_2O]_{out}+[NO_2]_{out}}{[NO]_{in}+[NH_3]_{in}} \times 100\%$$

Where $[NO]_{in}$ and $[NO]_{out}$ represent the inlet and outlet concentrations of gaseous NO; $[NH_3]_{in}$ is the inlet concentration of NH_3; $[N_2O]_{out}$ and $[NO_2]_{out}$ are the outlet concentrations of N_2O and NO_2, respectively.

2.3 Catalyst characterization

The BET surface areas of the samples were measured by N_2 adsorption at 77K using an Autosorb-1-C (Quantachrome Instrument Crop.). Powder X-ray diffraction (XRD) measurements were carried out on a Rigaku D/max 2550 PC system with Cu Kα radiation, and crystalline phases were identified by comparison with the reference data from International Center for Diffraction Data (ICDD) files. ICP with an IRIS Intrepid II apparatus were collected to analyze chemical compositions of the catalysts.

X-ray photoelectron spectroscopy (XPS) data were recorded on a Thermo ESCALAB 250 using Al Kα X-ray (hν = 1486.6 eV) as a radiation source at 150 W, calibrated by carbon deposit C 1s binding energy (BE) of 284.8 eV. Deconvolution of the peaks were performed after subtraction of the Shirley background using a sum of Lorentzian/Gaussian functions. Temperature programmed reduction of H_2 (H_2-TPR) was carried out on a chemisorption analyzer (Micromeritics, AutoChem II 2920) under 10% of H_2 in argon. The flow rate was 30 ml/min and temperature was increased from 100 to 900 ˚C at a rate of 10 ˚C/min.

Temperature programmed desorption of NH_3 (NH_3-TPD) was conducted in the same fixed-bed quartz reactor as that used in the activity tests. 400 mg of each catalyst was loaded in the reactor and

preheated at 350 ˚C in 800 ml/min N_2 for 2 h as the pretreatment. Samples were then cooled down to 100 ˚C and exposed to a 500 ml/min flow with 800 ppm NH_3 in the N_2 gas for 1 h. After that, a 500 ml/min N_2 purge was performed to sweep the physisorbed NH_3 and the temperature was elevated from 100 ˚C to 500 ˚C at a rate of 5 ˚C/min. The desorbed NH_3 was continually monitored by the Gasmet DX-4000 FT-IR detector.

In-situ diffuse reflectance infrared Fourier transform spectroscopy (DRIFTS) were recorded on a Nicolet 6700 spectrometer equipped with a Harrick IR cell and an MCT detector cooled by liquid N_2. Prior to each in-situ DRIFTS test, pretreatments were carried out and catalysts were heated up to 400 ˚C under a flow of 100 ml/min for 1 h to remove adsorbed impurities. The background spectrum was collected in the flowing N_2 and subtracted from the sample spectra. The spectra were recorded by accumulating 8 scans (for the transient NO+O_2 adsorption) or 32 scans (for other in-situ DRIFTS) at a resolution of 4 cm^{-1}. In order to diminish the influence of absorbance from different samples, the absorbance intensity was set to 2.50 for every sample at 400 ˚C.

3 Results and Discussion

3.1 SCR activity and resistance to Na-poisoning

SCR activities of samples with different $Ce(SO_4)_2$ content were compared and the results are presented in Figure 1. For both NO conversion and N_2-selectivity, it is found that the optimal mole ratio of V and $Ce(SO_4)_2$ is 1/0.5. In the following tests are focused on the V-0.5$Ce(SO_4)_2$/Ti sample (signed as V-$Ce(SO_4)_2$/Ti below for brevity) to study catalytic properties and reaction mechanism in comparison with the commercial V-W/Ti catalysts.

For a better display, Figure 2 (a) presents the activity comparison of fresh and Na-poisoned samples. It is obvious that V-$Ce(SO_4)_2$/Ti shows a higher NO conversion than the fresh commercial

V-W/Ti catalyst at low temperature (≤ 300 ˚C). For example, at 250 ˚C, V-Ce$(SO_4)_2$/Ti shows a conversion of 64% whereas that of the commercial sample is only 35%. When loading 0.5 wt% of Na, both samples are poisoned and NO conversions decline distinctly in the whole temperature range. Compared to the commercial catalyst, however, V-Ce$(SO_4)_2$/Ti exhibits a much better resistance to Na-poisoning since its NO conversion remains 77% while that of V-W-Na/Ti declines to only 50% at 400 ˚C. Having such good SCR activity and alkali resistance, V-Ce$(SO_4)_2$/Ti seems to have a potential as an effective NH_3-SCR catalyst, especially under high-Na containing conditions. Figure 2 (b) shows the N_2-selectivity: it is apparent that the N_2-selectivity of V-Ce$(SO_4)_2$/Ti starts to decrease above 300 ˚C. However, considering that temperature of SCR systems for coal-fired power plants is always not higher than 400 ˚C, the N_2-selectivity of 97% at 350 ˚C and 93% at 400 ˚C on V-Ce$(SO_4)_2$/Ti are still acceptable.

3.2 Effect of SO_2 and H_2O

As we mentioned in the Introduction part, SO_2 is an essential restriction to the application of CeO_2 based catalysts. It is therefore necessary to evaluate the effect of SO_2 on the SCR activity of V-Ce$(SO_4)_2$/Ti and V-Ce$(SO_4)_2$-Na/Ti. To better mimic the real exhaust gas, the effect of H_2O was also investigated. In our experiments, the activity at 350 ˚C was firstly chosen, since 350 ˚C is a typical operating temperature of coal-fired power plants SCR systems [12]. Besides, the durability test was also performed at 300 ˚C to assess the effect of SO_2 and H_2O in the low-T range, since V-Ce$(SO_4)_2$/Ti exhibited an obvious improvement in the activity tests at low temperatures (≤ 300 ˚C, Figure 2). Before adding SO_2 and H_2O, the SCR reactions had been stabilized for about 60-90 min. Then 500 ppm SO_2 and 5 % H_2O were added to the feed stream and such conditions were held for 10 h. After that, SO_2 and H_2O were removed from the feed stream and the reactions proceeded for

another 1 h.

As displayed in Figure 3 (a), NO conversion at 350 ˚C always keeps at 100% whether in the presence of SO_2 and H_2O or not. It seems that SO_2 and H_2O are not harmful to V-Ce$(SO_4)_2$/Ti. Actually, this good SO_2-tolerance is within expectation because it is known that V/Ti catalysts are stable in the presence of SO_2 [2]. As for Ce, the additive we used here is Ce$(SO_4)_2$, which is already a sulfated form and thus will not be poisoned by SO_2. At the lower temperature of 300 ˚C, V-Ce$(SO_4)_2$/Ti is not seriously affected by the presence of SO_2 and H_2O as well. As shown in Figure 3 (b), even though at the beginning of the SO_2 and H_2O addition, the NO conversion decreases from 97% to 84%, which could be due to the competitive adsorption of H_2O and NH_3 [6, 9], it then gradually recovers to 97 % with the continuous SO_2 and H_2O feeding. This recovery possibly should be attributed to the enhanced surface acidities from the SO_2 sulfuration [12, 16], providing more NH_3 adsorbing sites and to some extent offsetting the H_2O effect. Similar NO conversion increment is also found in the durability test of V-Ce$(SO_4)_2$-Na/Ti at 350 ˚C (see Figure S1 in the Support Information). After the addition of SO_2 and H_2O, NO conversion increases from 63% to 93%, which again, should be related to the acidity enhancement from the SO_2 sulfuration and “repair” the acidity damage by Na loading.

Therefore, the good SCR performance, alkali resistance and durability in the presence of SO_2 and H_2O make V-Ce$(SO_4)_2$/Ti to have prospects in practical NH_3-SCR applications.

3.3 Structure analysis

The BET surface areas of various catalysts are summarized in Table 1. For a better elucidation, samples with different Ce$(SO_4)_2$ contents are listed here. After Na loading, the BET surface area of V-W/Ti declines, which could be due to pore blocking by Na salts and can be one of the reasons for

the Na deactivation. Better stability is shown by the $Ce(SO_4)_2$ samples and no change appears after Na-poisoning. However, compared with the commercial catalyst, BET surface areas of the $Ce(SO_4)_2$ samples are evidently smaller and further decease with increasing $Ce(SO_4)_2$ content. This could be attributed to surface blocking by sulfates [12] and seems to correlate with the poor activity of samples with high $Ce(SO_4)_2$ content (Figure 1). Again, V-$Ce(SO_4)_2$/Ti in the following texts represents the samples with the ratio of 0.5, as emphasized above.

Figure 4 shows the XRD patterns of different catalysts. The anatase phase dominates on all the four samples and traces of rutile phase are also detected on the two $Ce(SO_4)_2$ doped ones [14], which should be due to the 15% rutile phase in P25. It is clear that Na doping does not change the crystalline structure of these catalysts. Besides, no crystalline V_2O_5 or CeO_2 is found, indicating the highly dispersed states of V and Ce [14]. Further researches need to be conducted to reveal the mechanism of the better performances observed with $Ce(SO_4)_2$.

3.4 Redox properties

XPS analysis was performed to investigate the atomic environment of the samples. Figure 5 (a) shows Ce 3d patterns of the fresh and Na-poisoned V-$Ce(SO_4)_2$/Ti. The spectra were fitted into 8 peaks and the two sub-bands labelled in orange represent the $3d^{10}4f^1$ state of Ce^{3+} cations, whereas the other ones labelled in blue correspond to the $3d^{10}4f^0$ of Ce^{4+} cations [14, 18]. It is reported that the Ce^{4+}/Ce^{3+} redox couple is promotional for the NH_3-SCR activity and Ce^{3+} could originate charge unbalance, vacancies and unsaturated chemical bonds on the catalyst surface, which results in a higher proportion of surface active oxygen and better redox properties [6, 7, 19]. Ce^{3+} ratios are calculated as the integral areas of $Ce^{3+}/(Ce^{3+}+Ce^{4+})$ and listed in Table 2. Evidently, the Ce^{3+} ratio declines from 49.24% to 15.19% after Na-poisoning, which is attributed to the electron transfer from

Na to the orbit of cerium oxide [18]. This lowers the favorability of oxygen vacancy creation and will cause a decrease in the proportion of Ce^{3+} according to Du's DFT results [18]. Therefore, doping with Na diminishes Ce^{3+} ratios and could hence influence the redox property of V-Ce$(SO_4)_2$/Ti, which results in the deactivation.

O 1s spectra of the four samples were also studied and shown in Figure 5(b). O 1s bands can be fitted into two peaks, referred to as the lattice oxygen at 530.3-530 eV (O_β) and the surface active oxygen at 532-531.6 eV (O_α) [8, 14]. O_α is thought to be more reactive in oxidation reactions due to its higher mobility. In fact, many researchers consider that high O_α ratio is beneficial for the NO oxidation in SCR reactions [7-9]. Herein, O_α ratios are calculated from $O_\alpha/(O_\alpha+ O_\beta)$ and listed in Table 2. Among four samples, fresh V-Ce$(SO_4)_2$/Ti has the highest O_α ratio of 28.80%, compared to 23.06% of the fresh V-W/Ti and around 20% of the two poisoned samples. Combining the results of Ce 3d patterns, the high O_α ratio should be related to the introduction of cerium, especially that of the Ce^{3+}. This enhancement is considerably important for the SCR activity at low temperatures, where the NO oxidative activation is crucial [1, 20]. After Na-poisoned, O_α ratios of the two fresh samples decrease, indicating the damage of redox properties by alkali metals, in agreement with other works [18, 21]. However, Na-poisoned V-Ce$(SO_4)_2$/Ti still has a relatively higher O_α ratio (21.93%) than V-W-Na/Ti (19.58%), which means that better redox properties remain and should contribute to its better performance in the activity tests.

Figure 6 shows the H_2-TPR results of four samples within the range of 100-900 ˚C. Peaks at 439 ˚C appear on the two fresh samples. For V-W/Ti, it is attributed to the overlap of V^{5+} to V^{3+} and W^{6+} to W^{4+} which is in the vicinity of surface vanadium oxide species [12, 22]. As for V-Ce$(SO_4)_2$/Ti, this peak should belong to the combination of V^{5+} to V^{3+}, Ce^{4+} to Ce^{3+} and related surface oxygen [14,

18]. Obviously, this peak is much more intense on the fresh V-Ce$(SO_4)_2$/Ti than on the commercial catalyst. For a better evaluation, 439 ˚C peaks are integrated and listed in Table 2. Note that the peak area could refer to reduction rates (i.e., H_2 consumption rates), since the temperature ranges of the two peaks at 439 ˚C are similar and temperatures were increased in a linear ramp at 10 ˚C/min. Thus, the double area of V-Ce$(SO_4)_2$/Ti indicates a much faster H_2 reduction at 439 ˚C, which correlates with the addition of Ce and the higher O_α ratio. It is also reasonable to speculate that the much faster H_2 reduction here would contribute to a stronger NO oxidative activation under SCR conditions, which will be discussed below. Reduction peaks at around 800 ˚C are observed on the two W-containing samples and assigned to W^{4+} to W^0 [22]. After Na doping, the main reduction peaks at 439 ˚C shift to higher temperatures on both samples. On V-W-Na/Ti, a broad band centered at 504 ˚C is observed, implying the damage of redox properties owing to the effect of Na, coincidence with the XPS analysis above. Whereas on V-Ce$(SO_4)_2$-Na/Ti, multiple peaks are detected and it is difficult to give an exact assignment to each one, since the reduction temperature of V and Ce is rather close [7]. But what is clear here is that an evident peak at 472 ˚C exists on V-Ce$(SO_4)_2$-Na/Ti, indicating that relatively better redox properties are still preserved, which accords with the XPS conclusions as well.

3.5 Surface acidity

Surface acidity is another essential factor in NH_3-SCR reactions. In order to investigate such properties, NH_3-TPD runs were performed on the four samples: the TPD profiles are shown in Figure 7, while integrals of the curves, which represent total surface acidities, are listed in Table 3 (for a direct comparison, normalized by the value of V-W/Ti). Weak and strong acidities are also identified in the TPD profiles based on the temperature regions. Peaks below 200 ˚C can be assigned to the maxima of NH_3 desorption from weakly acid sites, while those higher than 300 ˚C are attributed to

the strong acid sites [14, 23]. From Figure 7, both the weak and strong acidities of V-Ce$(SO_4)_2$/Ti are stronger than those of the commercial V-W/Ti, which results in a 30% increment of total acidity (1.30 vs. 1). As it is widely accepted that NH_3 should firstly adsorb on catalysts surface and then participate in the SCR reaction [24-26], the stronger surface acidities of V-Ce$(SO_4)_2$/Ti could thus contribute to its better SCR activity. After Na loading, total acidities apparently decrease on both samples, including partial weak and most of strong acidities, which is in accordance with other works about alkali metals deactivation [5, 11]. When the two Na-poisoned catalysts are compared, it is obvious that V-Ce$(SO_4)_2$-Na/Ti has more abundant acidities (0.81 vs. 0.33): especially moderately strong acid sites are preserved, which should be related to its favorable Na-resistance effect.

To study the nature of surface acid sites, in-situ DRIFTS spectra during NH_3 adsorption/desorption were collected over the four catalysts from 100 ˚C to 400 ˚C and shown in Figure 8. Bands at 1600 cm^{-1}, 1300-1150 cm^{-1} and 3400-3100 cm^{-1} are assigned to NH_3 adsorption on Lewis acid sites, while those at about 1673 cm^{-1} and 1435 cm^{-1} belong to NH_4^+ on Brønsted acid sites [12, 27]. Two negative peaks centered at around 3650 cm^{-1} and 1370 cm^{-1} are observed on the two fresh samples as well, due to NH_3 adsorption on the V-OH sites and O=S=O of surface SO_4^{2-} respectively [12, 25]. After partial NH_3 desorption, bands at 1343-1332 cm^{-1} assigned to coordinated SO_4^{2-} appear [28, 29], indicating that some occupied SO_4^{2-} sites start to be released. To better investigate the two types of acidities, integration of peaks at ~ 1435 cm^{-1} (for Brønsted sites) and 1300-1150 cm^{-1} (for Lewis sites) at 100 ˚C was performed [30]. Besides, bands of V-OH and SO_4^{2-} are also integrated to analyze the V and SO_4^{2-} sites, respectively. All the integration results are displayed in Table 3 and normalized by the relevant values of the commercial V-W/Ti sample.

From Table 3, it is clear that V-Ce$(SO_4)_2$/Ti shows a much stronger NH_4^+ adsorption on Brønsted

sites (3.37 times of V-W/Ti), accompanied with more distinct negative bands of O=S=O, which can be interpreted since SO_4^{2-} has been verified to provide strong Brønsted acid sites after loading on catalysts [12, 13]. These results agree well with the NH_3-TPD curves in Figure 7 and could explain the acidity increment of V-Ce$(SO_4)_2$/Ti. Moreover, some O=S=O negative bands are also detected on the commercial V-W/Ti, which is attributed to its moderate sulfur content (confirmed by XPS spectra of S 2p, shown in Figure S2 in the Support Information). Actually, commercial SCR catalysts always contain about 0.5-1% of sulfur, which mostly exists in the form of surface sulfates, due to the preparation method of TiO_2 [13]. Besides, almost the same amount of V-OH sites are observed on the two fresh samples (1 vs. 1.04), indicating that these two catalysts have comparable V contents.

After Na poisoning, both Lewis and Brønsted acidities decrease severely on the two samples. In fact, from Table 3, Lewis acidities of V-W/Ti and V-Ce$(SO_4)_2$/Ti decline about 60% and 40%, respectively. The Brønsted sites decline even more significantly and only about 25% resist on both samples. These results explain the drop of total acidities in the NH_3-TPD curves and indicate that the more abundant Lewis and Brønsted acid sites preserved on V-Ce$(SO_4)_2$-Na/Ti should support its good performance in the SCR activity tests.

In addition to the adsorbed NH_3 species, V-OH and SO_4^{2-} sites also need to be analyzed. As displayed in Table 3, most of the V-OH is destroyed after Na poisoning and such a damage could result in deactivation, since V-OH is thought to be the active sites for the NH_3-SCR reactions [24, 25]. Besides, O=S=O peaks at ~ 1370 cm^{-1} vanish and negative bands in the range of 1350-1300 cm^{-1} emerge on both poisoned samples, assigned to NH_3 adsorption on the chelating bidentate “inorganic” SO_4^{2-} with ionic S-O bonds [28, 31]. It seems that partial O=S=O sites transform into these “inorganic” SO_4^{2-} under the effect of sodium, because alkali metals are reported to be able to cause

extension of bonds length and thus originate the red shift of vibration frequency [5, 21]. As a result, this interaction between Na and SO_4^{2-} could act as a protection of the V-OH sites, leading to a relatively higher V-OH content remaining on V-Ce$(SO_4)_2$-Na/Ti (0.33 vs. 0.26), and therefore contributing to its better SCR activity.

3.6 In-situ DRIFTS of TPSR

Extensive in-situ DRIFTS spectra of TPSR (temperature programmed surface reaction) runs were carried out to study the reaction mechanism over V-Ce$(SO_4)_2$/Ti. Since its promotional effect on SCR activity is mainly below 300 ˚C, and also considering the stability of reaction intermediates, we focused on the reactions at 250 ˚C, where a maxima increment of NO conversion is observed in Figure 2 (a). In each TPSR experiment, samples were firstly exposed to a 100 ml/min flow of 1000 ppm NH_3 for 1 h and then purged by N_2 for 30 min to remove the physisorbed NH_3. Afterwards, 1000 ppm NO + 5 % O_2 were introduced and the temporal evolution of DRIFTS spectra was recorded. Reverse procedures were performed for the reactions between NH_3 and adsorbed NO+O_2 species. For a better comparison, the same tests were also performed over commercial V-W/Ti, V-W-Na/Ti and V-Ce$(SO_4)_2$-Na/Ti.

3.6.1 Reaction between NO+O_2 and adsorbed NH_3 species

Figure 9 shows the in-situ DRIFTS spectra of reactions between NO + O_2 and adsorbed NH_3 species recorded in TPSR runs at 250 ˚C. Bands that are very similar to those in Figure 8 can be observed and their assignments are the same. It is obvious that NH_3 adsorption on V-Ce$(SO_4)_2$/Ti is much stronger than on commercial V-W/Ti and the two Na-poisoned samples, which is in agreement with the in-situ DRIFTS of NH_3-TPD results above. Furthermore, these surface NH_3 species on

V-Ce$(SO_4)_2$/Ti are more reactive since the larger bands of adsorbed NH_3 diminish faster after NO+O_2 introduction, while the smaller ones associated with NH_3 adsorption on V-W/Ti show a much slower decrease (integration of NH_4^+ bands at 1432 cm^{-1} and consumption ratios are listed in Table 4), in line with the activity results at 250 ˚C. Also, the negative bands of O=S=O decrease evidently with the introduction of NO+O_2, indicating that SO_4^{2-} sites are reactive in the SCR reaction as well. For the two Na-poisoned samples, no NH_4^+ but only some Lewis bonded NH_3 bands at 1602 cm^{-1} and at around 1226 cm^{-1} can be detected. In fact, the peaks at 1602 cm^{-1} exit almost during the entire exposure to NO+O_2, comparing to their depletion within 10 min of NO+O_2 introduction to the two fresh samples and referring to the decreased reactivity between NO+O_2 and adsorbed NH_3 after Na poisoning.

When most of the surface NH_3 is consumed, new bands at ~1616 cm^{-1} appear on the two fresh samples. After the complete NH_3 depletion, traces of peaks at 1375-1380 cm^{-1} can be detected. These bands are not observed in the NH_3-TPD spectra and thus should be related to NO+O_2. According to the literature, bands at 1375-1380 cm^{-1} are attributed to the free nitrate ions (NO_3^-) [27, 32], whereas the assignments of those at ~ 1616 cm^{-1} are controversial: Peng et al. [7] recorded in-situ DRIFTS spectra of NO + O_2 exposed to VOx/CeO_2 nanorods and assigned the bands at 1610 cm^{-1} to adsorbed NO_2. Similarly, Liu et al. [14] observed bands at 1613 cm^{-1} in their in-situ DRIFTS spectra of NO + O_2 adsorption on V_2O_5-CeO_2/TiO_2 and also assigned them to adsorbed NO_2. While in a more recent study of NO oxidation over Cu-CHA, Ruggeri et al. [33] attributed the bands at 1620 cm^{-1} to bridging nitrates. Since our samples are also vanadium oxides and closer to the two former cases, attribution of the bands at 1616 cm^{-1} to adsorbed NO_2 appears more in line with our experimental results. However, it is worth mentioning that either adsorbed NO_2 or bridging nitrates should come

from the NO oxidative activation, and formation of such species is a signature of the catalysts redox properties. In the following part, we mainly attribute these 1616 cm^{-1} bands to adsorbed NO_2.

3.6.2 Reaction between NH_3 and adsorbed $NO+O_2$ species

In this part, firstly $NO+O_2$ adsorption on the four samples and then reaction with NH_3 were conducted to confirm the formation of adsorbed NO_2 and NO_3^-, and also to investigate the reactivity of these oxidized NOx species. Figure 10 shows in-situ DRIFTS spectra of TPSR runs at 250 ˚C. After $NO+O_2$ treatment, adsorbed NO_2 at ~ 1616 cm^{-1} and NO_3^- at around 1380 cm^{-1} are detected over the two fresh catalysts, confirming that these two species come from the oxidation of NO. However, in the two Na-poisoned cases, no such oxidized NOx species can be observed, indicating the damage of redox properties by Na loading and in agreement with the characterization results above. Furthermore, the NO_3^- bands on V-Ce$(SO_4)_2$/Ti are obviously larger than on the commercial catalyst, inferring an abundance of nitrates on the Ce$(SO_4)_2$ sample. This could be attributed to the favorable redox properties of V-Ce$(SO_4)_2$/Ti and thus points to a stronger NO oxidation, as we mentioned in section 3.4, which contributes to its better low-T activity.

As soon as NH_3 is introduced, all the NO_3^- bands disappear, implying that there is no co-existence of NO_3^- and adsorbed NH_3 at 250 ˚C in our case. This could be due to the reaction between NO_3^- and NH_3 producing NH_4NO_3 and then decomposition at 250 ˚C [1, 26]. Alternatively, the NO_3^- may also be directly reduced by NH_3 to N_2, which is the mechanism proposed by Grossale et al. [34] for the NO_2 SCR reaction. Both the two reaction pathways could be possible. After NH_3 purging for 30 min, four samples exhibit similar results as those after NH_3 adsorption in Figure 9, again, confirming the better acidity of V-Ce$(SO_4)_2$/Ti. Thus, these two TPSR experiments verify the reactivity of the abundant surface acidities on V-Ce$(SO_4)_2$/Ti and also reflect its good redox properties for the NO

oxidative activation.

3.7 Transient $NO+O_2$ adsorption and mechanism proposal

In order to elucidate the NO activation mechanism at 250 ˚C, transient $NO+O_2$ adsorption experiments were performed. In this experiment, pretreatment was conducted in an oxidative atmosphere with 5 % O_2 at 400 ˚C to obtain an oxidized state. Figure 11 (a) - (d) show the temporal evolution of DRIFTS spectra. Since the signals of bands centered at 2240 cm^{-1} are rather weak, we have to magnify the 2450 – 2050 cm^{-1} region, displayed in Figure 11 (c) and (d), to enable a closer analysis of this portion of the spectra. As discussed above, peaks at 1612 cm^{-1} and 1375 cm^{-1} are related to adsorbed NO_2 and NO_3^- respectively, whereas the bands in the range of 2240 - 2140 cm^{-1}, according to the literature [35], are assigned to NO^+ species. The formal oxidation state of nitrogen atom in NO^+ is +3, so that it can be identified as a nitrite-like species or the precursor of a nitrite, which is widely accepted as the reactive intermediate in NH_3 SCR reactions [1, 20, 33, 36]. To show the dynamics of these species, integral areas of the relative bands are compared in Figure 12 (a) and (b). Integration of 2240 cm^{-1} bands on V-W/Ti is not performed since the signals are extremely slight, and can be seriously affected by the noise.

It is evident that upon $NO+O_2$ introduction, peaks at ~ 1613 cm^{-1} and 1375 cm^{-1} appear simultaneously but grow at different rates on the two samples. Comparing the integral areas in Figure 12 (a) and (b), in the first 30 s relatively higher amounts of adsorbed NO_2 and NO_3^- are formed on V-$Ce(SO_4)_2$/Ti, indicating its better redox properties. In the first 1.5 min, the amount of adsorbed NO_2 is similar (labelled by blue dotted line), while NO_3^- formation is much more distinct on V-$Ce(SO_4)_2$/Ti (labelled by red dotted line). As for the NO^+ species, its formation on V-$Ce(SO_4)_2$/Ti, by direct comparison of Figure 11 (c) and (d), is much more apparent than that on V-W/Ti. As

accepted by many researchers [1, 20, 36-39], the standard SCR mechanism at low temperature is strongly related to the oxidative activation of NO, proposed to be oxidized into nitrites (NO_2^-) or nitrite-like NO^+ species, which then readily react with adsorbed NH_3 species and decompose into N_2 and H_2O:

$$NO_2^- + NH_3* + H^+ \rightarrow [NH_4NO_2] \rightarrow N_2 + H_2O \quad (1)$$

$$NO^+ + H_2O \leftrightarrow H^+ + HONO \quad (2)$$

$$HONO + NH_3* \rightarrow [NH_4NO_2] \rightarrow N_2 + H_2O \quad (3)$$

When there is no NH_3, nitrites and NO^+ species can be further oxidized to nitrates [33, 39, 40], which is a more stable species and is clearly detected in our experiments. Thus, the much more abundant nitrates and NO^+ species formation on V-Ce$(SO_4)_2$/Ti indicates its better redox properties and stronger NO oxidative activation. Combining the XPS and H_2-TPR results above, this stronger NO oxidative activation coincides with the higher ratio of surface active oxygen and larger H_2 consumption at low temperature on V-Ce$(SO_4)_2$/Ti, as we proposed before, and hence contributes to its higher NO conversion at 250 ˚C.

As for the adsorbed NO_2, it could come from the nitrates reduction by NO, which is reported to occur at temperature as low as 170 ˚C [1, 39]:

$$NO + NO_3^- \leftrightarrow NO_2 + NO_2^- \quad (4)$$

Alternatively, adsorbed NO_2 could also come from the direct NO oxidation, which, however, is rather limited over V-based catalysts [2] and therefore may not contribute significantly to the adsorbed NO_2 formation here.

After 1.5 min, on V-Ce$(SO_4)_2$/Ti, adsorbed NO_2 is less while the content of surface NO_3^- is much higher than on V-W/Ti. This might be due to the NO_3^- agglomeration on V-Ce$(SO_4)_2$/Ti which blocks

its surface sites so that NO_2 adsorption is inhibited. Besides, the increase of NO^+ species is quite slow, which may relate to the NO^+ oxidation into NO_3^- with the cost of adsorbed NO_2 [33]. After 3 min of $NO+O_2$ introduction, adsorbed NO_2 begins to decrease on both samples and V-W/Ti decreases intensely. The adsorbed NO_2 can desorb into the gas phase and some of it also disproportionates to form NO_3^- via the well-known NO_2 disproportionation [1, 39], confirmed by the slight increment of NO_3^- until 7 min on V-W/Ti. After that, NO_3^- decreases slowly on the commercial catalyst while adsorbed NO_2 increases slightly, which could be due to the NO_3^- reduction by NO, i.e. reaction (4). On V-$Ce(SO_4)_2$/Ti, however, evolution of adsorbed NO_2 and NO_3^- is contrary to what happens on V-W/Ti after 7 min. It seems that NO_2 disproportionation to NO_3^- is primary in this case, indicated by the simultaneous NO^+ species increasing. Actually, when there is NH_3, reaction (1) - (3) proceed readily so that no obvious NO_3^- or adsorbed NO_2 can accumulate on the catalyst surface, as verified by Figure 9: only after most of the adsorbed NH_3 is depleted, can these oxidized NOx species be detected. Consequently, combining the results above, we can conclude that the better redox properties of V-$Ce(SO_4)_2$/Ti result in a much stronger NO oxidative activation, which is verified by the characterization results and by the abundant formation of NO^+ and NO_3^- species. When exposed to SCR conditions where both NH_3 and NO exist, this stronger NO oxidative activation produces more reactive nitrite and/or nitrite-like intermediates which then readily react with the adsorbed NH_3 species via reaction (1) – (3), and could thus account for the improved activity of V-$Ce(SO_4)_2$/Ti observed at low temperatures.

4 Conclusions

A series of V-$Ce(SO_4)_2$/Ti catalysts are prepared by impregnation method for the selective catalytic reduction of NO with NH_3. The optimal mole ratio of V and $Ce(SO_4)_2$ is 1/0.5 and both the low-T

activity and the alkali resistance of V-0.5Ce$(SO_4)_2$/Ti are found to be better than on the commercial V-W/Ti catalyst. It is also noticed that V-0.5Ce$(SO_4)_2$/Ti shows an excellent durability in the presence of SO_2 and H_2O, which indicates favorable prospects for its industrial application since real exhaust gas always contains large amounts of SO_2 and H_2O. In order to reveal the mechanism of such promotional effects, both an extensive characterization and an in-situ DRIFTS investigation are carried out. Higher proportion of surface active oxygen generated by the introduction of Ce and much faster H_2 reduction are observed on V-0.5Ce$(SO_4)_2$/Ti, contributing to its better redox properties and to the more abundant formation of surface NO^+ and NO_3^- species. When exposed to both NH_3 and NO under SCR conditions, a stronger NO oxidative activation will promote formation of more nitrite and/or nitrite-like NO^+ reactive intermediates, which can readily react with the adsorbed NH_3 species to produce N_2 and H_2O, thus accounting for the improved SCR activity of V-0.5Ce$(SO_4)_2$/Ti at low temperatures.

After Na poisoning, the improved redox properties and surface acidity still remain on V-0.5Ce$(SO_4)_2$-Na/Ti, and also more V-OH sites are preserved owing to the interaction between Na and O=S=O, which acts as a protection for the active sites. These promotional effects contribute to the enhanced alkali resistance of V-0.5Ce$(SO_4)_2$/Ti. Therefore, all the results in this study suggest that V-0.5Ce$(SO_4)_2$/Ti is a promising candidate as a catalyst for NH_3-SCR in coal-fired power plants, especially under high Na-content conditions.

Acknowledgements

The authors wish to thankfully acknowledge Dr. Xuesen Du from the Key Laboratory of Low-Grade Energy Utilization Technologies and Systems of Ministry of Education of China, College of Power Engineering, Chongqing University, for his valuable contribution to results discussion.

This work is financially supported from the Key Research & Development Plan of Shandong Province (No. 2014GJJS0501), the Environmental Welfare Project of Ministry of Environmental Projection of China (No. 201509012), the National Science and Technology Support Program (No. 2015BAA05B02-2), the National Key research and Development Plan (No. 2016YFC0203701) and the National Science Foundation of China (No. 51306079).

Reference

[1] E. Tronconi, I. Nova, C. Ciardelli, D. Chatterjee, M. Weibel, J. Catal. 245 (2007) 1-10.

[2] G. Busca, L. Lietti, G. Ramis, F. Berti, Appl. Catal. B: Environ. 18 (1998) 1-36.

[3] P. Forzatti, I. Nova, E. Tronconi, Angew. Chem. Int. Ed. 48 (2009) 8366-8368.

[4] J.P. Chen, M.A. Buzanowski, R.T. Yang, J.E. Cichanowicz, J. Air Waste Manage. 40 (1990) 1403-1409.

[5] X.S. Du, X. Gao, K.Z. Qiu, Z.Y. Luo, K.F. Cen, J. Phys. Chem. C 119 (2015) 1905-1912.

[6] R.Y. Qu, X. Gao, K.F. Cen, J.H. Li, Appl. Catal. B: Environ. 142 (2013) 290-297.

[7] Y. Peng, C.Z. Wang, J.H. Li, Appl. Catal. B: Environ. 144 (2014) 538-546.

[8] W.P. Shan, F.D. Liu, H. He, X.Y. Shi, C.B. Zhang, Appl. Catal. B: Environ. 115 (2012) 100-106.

[9] H. Chang, X. Chen, J. Li, L. Ma, C. Wang, C. Liu, J.W. Schwank, J. Hao, Environ. Sci. Technol. 47 (2013) 5294-5301.

[10] X.S. Du, X. Gao, L.W. Cui, Y.C. Fu, Z.Y. Luo, K.F. Cen, Fuel 92 (2012) 49-55.

[11] Y. Peng, J.H. Li, L. Chen, J.H. Chen, J. Han, H. Zhang, W. Han, Environ. Sci. Technol. 46 (2012) 2864-2869.

[12] W. Hu, X. Gao, Y. Deng, R. Qu, C. Zheng, X. Zhu, K. Cen, Chem. Eng. J. 293 (2016) 118-128.

[13] S.T. Choo, Y.G. Lee, I.S. Nam, S.W. Ham, J.B. Lee, Appl. Catal. A: Gen 200 (2000) 177-188.

[14] Z.M. Liu, S.X. Zhang, J.H. Li, J.Z. Zhu, L.L. Ma, Appl. Catal. B: Environ. 158 (2014) 11-19.

[15] L. Chen, J.H. Li, M.F. Ge, J. Phys. Chem. C 113 (2009) 21177-21184.

[16] D. Ye, R.Y. Qu, H. Song, X. Gao, Z.Y. Luo, M.J. Ni, K.F. Cen, Chem. Eng. J. 283 (2016) 846-854.

[17] L. Lietti, I. Nova, P. Forzatti, Top. Catal. 11-12 (2000) 111-122.

[18] X.S. Du, X. Gao, R.Y. Qu, P.D. Ji, Z.Y. Luo, K.F. Cen, Chemcatchem 4 (2012) 2075-2081.

[19] X. Gao, Y. Jiang, Y. Zhong, Z.Y. Luo, K.F. Cen, J. Hazard Mater. 174 (2010) 734-739.

[20] I. Nova, C. Ciardelli, E. Tronconi, D. Chatterjee, B. Bandl-Konrad, AIChE J. 52 (2006) 3222-3233.

[21] J. Due-Hansen, S. Boghosian, A. Kustov, P. Fristrup, G. Tsilomelekis, K. Stahl, C.H. Christensen, R. Fehrmann, J. Catal. 251 (2007) 459-473.

[22] P.G.W.A. Kompio, A. Bruckner, F. Hipler, G. Auer, E. Loffler, W. Grunert, J. Catal. 286 (2012) 237-247.

[23] Y. Jiang, X. Gao, Y.X. Zhang, W.H. Wu, H. Song, Z.Y. Luo, K.F. Cen, J. Hazard Mater. 274 (2014) 270-278.

[24] N.Y. Topsoe, Science 265 (1994) 1217-1219.

[25] N.Y. Topsoe, H. Topsoe, J.A. Dumesic, J. Catal. 151 (1995) 226-240.

[26] I. Nova, C. Ciardelli, E. Tronconi, D. Chatterjee, B. Bandl-Konrad, Catal. Today 114 (2006) 3-12.

[27] K.I. Hadjiivanov, Catal. Rev. 42 (2000) 71-144.

[28] F. Liu, K. Asakura, H. He, W. Shan, X. Shi, C. Zhang, Appl. Catal. B: Environ. 103 (2011) 369-377.

[29] Z. Topalian, G.A. Niklasson, C.G. Granqvist, L. Osterlund, ACS Appl. Mater. Interfaces 4 (2012) 672-679.

[30] Y. Peng, J.H. Li, X. Huang, X. Li, W.K. Su, X.X. Sun, D.Z. Wang, J.M. Hao, Environ. Sci. Technol. 48 (2014) 4515-4520.

[31] R.Q. Long, R.T. Yang, J. Catal. 186 (1999) 254-268.

[32] M.P. Ruggeri, T. Selleri, M. Colombo, I. Nova, E. Tronconi, J. Catal. 328 (2015) 258-269.

[33] M.P. Ruggeri, I. Nova, E. Tronconi, J.A. Pihl, T.J. Toops, W.P. Partridge, Appl. Catal. B: Environ. 166 (2015) 181-192.

[34] A. Grossale, I. Nova, E. Tronconi, Catal. Lett. 130 (2009) 525-531.

[35] Adrian Marberger, Davide Ferri, Martin Elsener, O. Krçcher, Angew. Chem. Int. Ed. 55 (2016) 1-7.

[36] J.H. Kwak, J.H. Lee, S.D. Burton, A.S. Lipton, C.H. Peden, J. Szanyi, Angew. Chem. Int. Ed. 52 (2013) 9985-9989.

[37] D. Wang, L. Zhang, K. Kamasamudram, W.S. Epling, ACS Catal. 3 (2013) 871-881.

[38] F. Gao, E.D. Walter, M. Kollar, Y.L. Wang, J. Szanyi, C.H.F. Peden, J. Catal. 319 (2014) 1-14.

[39] C. Ciardelli, I. Nova, E. Tronconi, D. Chatterjee, B. Bandl-Konrad, M. Weibel, B. Krutzsch, Appl. Catal. B: Environ. 70 (2007) 80-90.
[40] A. Grossale, I. Nova, E. Tronconi, D. Chatterjee, M. Weibel, J. Catal. 256 (2008) 312-322.

Table 1

Table 1. BET surface area of various catalysts

Samples	BET surface area (m^2/g)	Samples	BET surface area (m^2/g)
V-W/Ti	65.1	V-1Ce$(SO_4)_2$/Ti	42.2
V-W-Na/Ti	60.5	V-1Ce$(SO_4)_2$-Na/Ti	42.1
V-0.5Ce$(SO_4)_2$/Ti	48.1	V-2Ce$(SO_4)_2$/Ti	39.5
V-0.5Ce$(SO_4)_2$-Na/Ti	48.2	V-5Ce$(SO_4)_2$/Ti	26.2

Table 2

Table 2. Redox properties of the four samples

Samples	Ce^{3+}	Ce^{4+}	O_α	O_β	Peaks at 439 ˚C
V-$Ce(SO_4)_2$/Ti	49.24%	50.76%	28.80%	71.20%	1.40
V-$Ce(SO_4)_2$-Na/Ti	15.19%	84.81%	21.93%	78.07%	/
V-W/Ti	/	/	23.06%	76.94%	0.69
V-W-Na/Ti	/	/	19.58%	80.42%	/

Table 3

Table 3. Normalized integration area from NH_3-TPD and in-situ DRIFTS of NH_3-TPD

Samples	Total surface acidities	Lewis acidities [a]	Brønsted acidities [b]	V-OH [c]	SO_4^{2-} [d]
V-W/Ti	1	1	1	1	1
V-W-Na/Ti	0.33	0.43	0.24	0.26	0.19
V-$Ce(SO_4)_2$/Ti	1.30	0.81	3.37	1.04	2.03
V-$Ce(SO_4)_2$-Na/Ti	0.81	0.47	0.88	0.33	0.90

[a] Integrated from in-situ DRIFTS spectra at 100 ˚C, peaks in the range of 1300-1150 cm^{-1};

[b] Integration of peaks at around 1435 cm^{-1}, the same spectra as Lewis acidities.

[c] Integration of peaks centered at around 3650 cm^{-1}, spectra at 100 ˚C.

[d] Integration of the negative bands centered at around 1370 cm^{-1} for the fresh and 1350-1300 cm^{-1} for the poisoned.

Table 4

Table 4. Normalized integration area of NH_4^+ bands at 1432 cm^{-1} and consumption

Samples	After NH_3 adsorption [a]	Consumption after 10 min [b]	Consumption after 15 min
V-W/Ti	1	6%	48%
V-$Ce(SO_4)_2$/Ti	4.21	42%	97%

[a] Integrated from in-situ DRIFTS spectra after NH_3 adsorption and normalized by the value of V-W/Ti;

[b] Area variation after 10 min divided by area after NH_3 adsorption, the same in consumption after 15 min.

Figure captions

Figure 1. (a) Activity comparison of samples with different $Ce(SO_4)_2$ content. (b) N_2-selectivity of relevant samples. Reaction conditions: catalyst mass = 200 mg, [NO] = [NH_3] = 800 ppm, [O_2] = 5 vol.%, total flow rate = 500 mL/min, GHSV = 150,000 mL/g·h.

Figure 2. (a) Activity comparison of fresh and Na-poisoned samples. (b) N_2-selectivity of relevant samples. Reaction conditions: catalyst mass = 200 mg, [NO] = [NH_3] = 800 ppm, [O_2] = 5 vol.%, total flow rate = 500 mL/min, GHSV = 150,000 mL/g·h.

Figure 3. Effect of SO_2 and H_2O on the SCR activity of V-$Ce(SO_4)_2$/Ti at (a) 350 ˚C and (b) 300 ˚C. Reaction conditions: catalyst mass = 200 mg, [NO] = [NH_3] = 800 ppm, [O_2] = 5 vol.%, [SO_2] = 500 ppm (when used), H_2O = 5 vol.% (when used), total flow rate = 500 mL/min, GHSV = 150,000 mL/g·h.

Figure 4. XRD patterns of the fresh and Na-poisoned catalysts. (♣) Anatase TiO_2 and (♥) Rutile TiO_2.

Figrue 5. XPS spectra of (a) Ce 3d of two $Ce(SO_4)_2$ samples and (b) O 1s of the four samples.

Figure 6. H_2-TPR profiles of the four samples.

Figure 7. NH_3-TPD profiles of the four samples.

Figrue 8. In-situ DRIFTS spectra of NH_3-TPD over of the four samples. (a) V-W/Ti, (b) V-W-Na/Ti, (c) V-$Ce(SO_4)_2$/Ti and (d) V-$Ce(SO_4)_2$-Na/Ti.

Figure 9. In-situ DRIFTS spectra of reactions between NO+O_2 and adsorbed NH_3 species at 250 ˚C over (a) V-W/Ti, (b) V-$Ce(SO_4)_2$/Ti, (c) V-W-Na/Ti and (d) V-$Ce(SO_4)_2$-Na/Ti.

Figure 10. In-situ DRIFTS spectra of reactions between NH_3 and adsorbed NO+O_2 species at 250 ˚C over (a) V-W/Ti, (b) V-$Ce(SO_4)_2$/Ti, (c) V-W-Na/Ti and (d) V-$Ce(SO_4)_2$-Na/Ti.

Figure 11. In-situ DRIFTS spectra of transient NO+O_2 adsorption over (a) V-W/Ti, range of 1700-1200 cm^{-1}, (b) V-$Ce(SO_4)_2$/Ti, range of 1700-1200 cm^{-1}, (c) V-W/Ti, range of 2450-2050 cm^{-1}, and (d) V-$Ce(SO_4)_2$/Ti, range of 2450-2050 cm^{-1}.

Figure 12. Peak area dynamics of the related in-situ DRIFTS bands during the transient NO+O_2 adsorption over (a) VW/Ti, and (b) V-$Ce(SO_4)_2$/Ti.

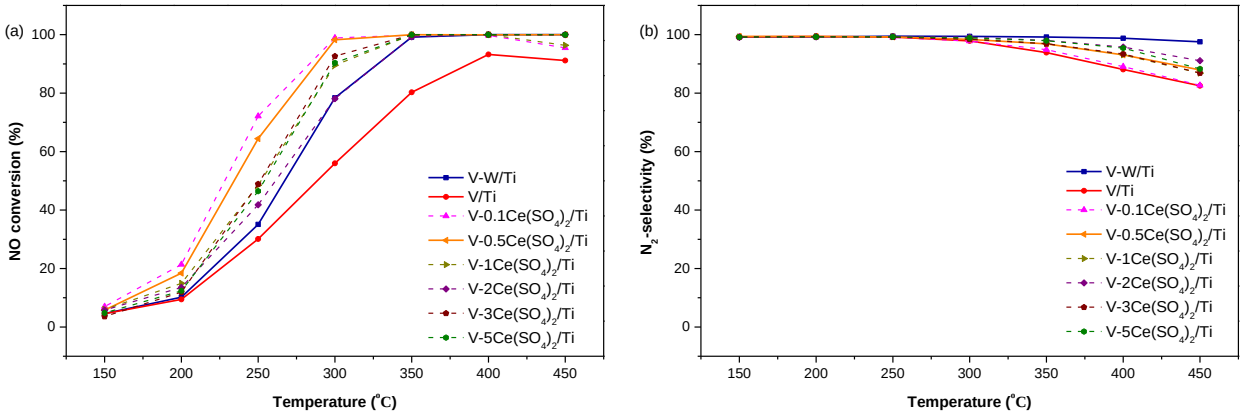

Figure 1. (a) Activity comparison of samples with different $Ce(SO_4)_2$ content. (b) N_2-selectivity of relevant samples. Reaction conditions: catalyst mass = 200 mg, [NO] = [NH_3] = 800 ppm, [O_2] = 5 vol.%, total flow rate = 500 mL/min, GHSV = 150,000 mL/g·h.

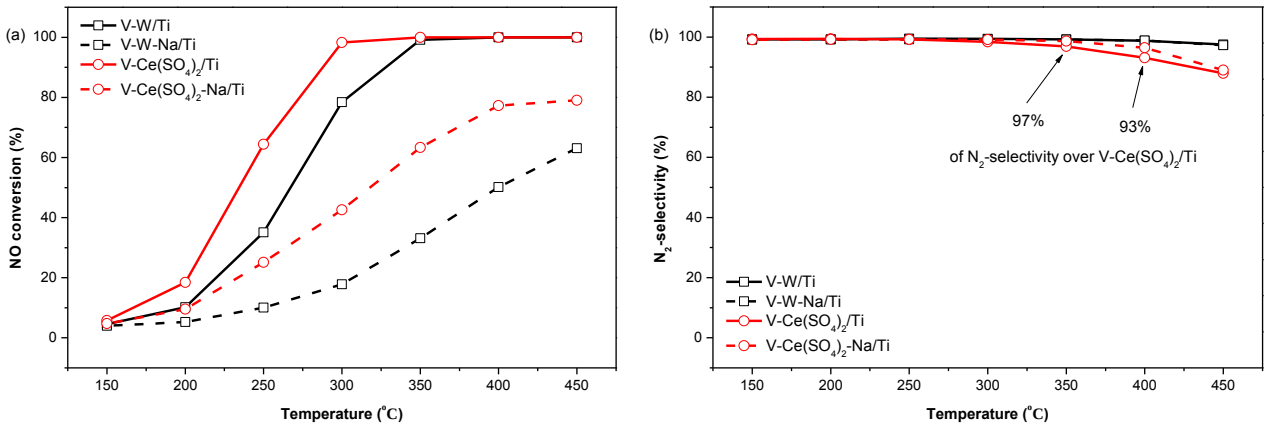

Figure 2. (a) Activity comparison of fresh and Na-poisoned samples. (b) N_2-selectivity of relevant samples. Reaction conditions: catalyst mass = 200 mg, [NO] = [NH_3] = 800 ppm, [O_2] = 5 vol.%, total flow rate = 500 mL/min, GHSV = 150,000 mL/g·h.

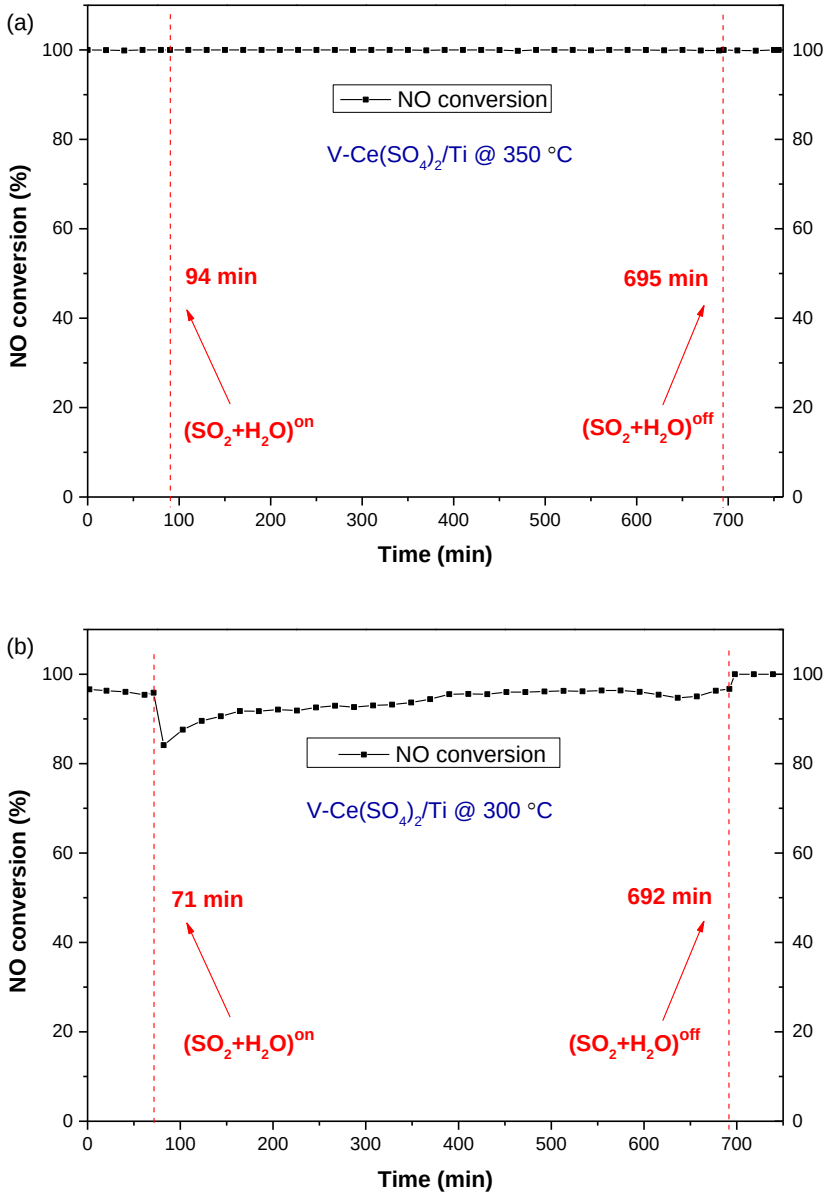

Figure 3. Effect of SO_2 and H_2O on the SCR activity of V-Ce$(SO_4)_2$/Ti at (a) 350 ˚C and (b) 300 ˚C. Reaction conditions: catalyst mass = 200 mg, [NO] = [NH_3] = 800 ppm, [O_2] = 5 vol.%, [SO_2] = 500 ppm (when used), H_2O = 5 vol.% (when used), total flow rate = 500 mL/min, GHSV = 150,000 mL/g·h.

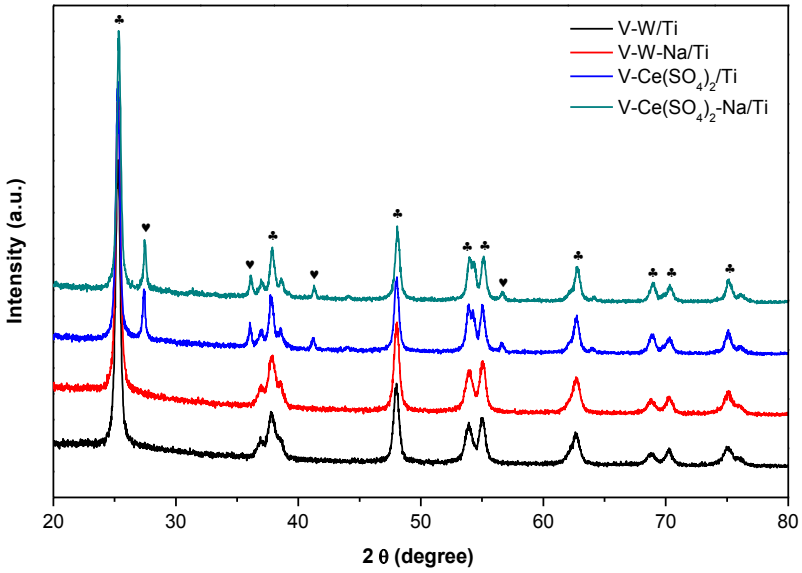

Figure 4. XRD patterns of the fresh and Na-poisoned catalysts. (♣) Anatase TiO_2 and (♥) Rutile TiO_2.

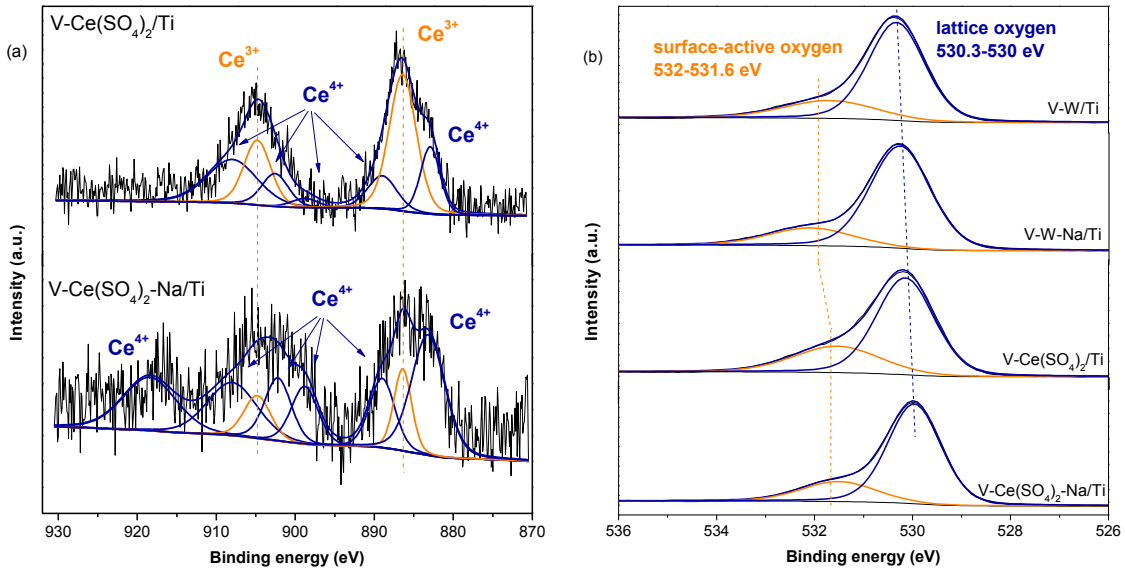

Figure 5. XPS spectra of (a) Ce 3d of two $Ce(SO_4)_2$ samples and (b) O 1s of the four samples.

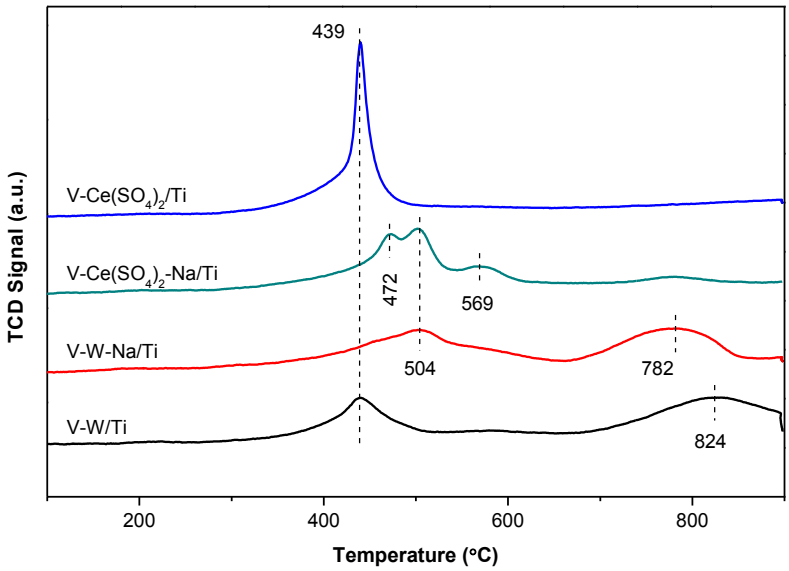

Figure 6. H_2-TPR profiles of the four samples

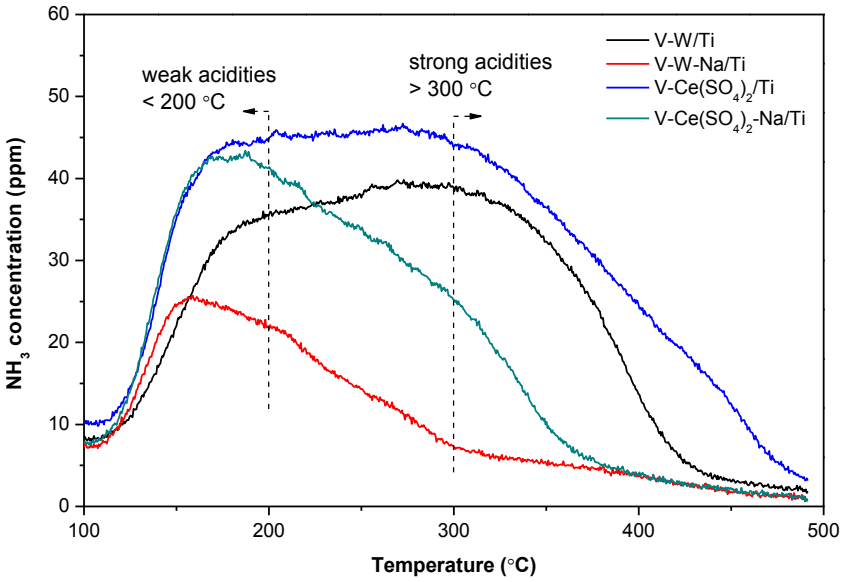

Figure 7. NH_3-TPD profiles of the four samples

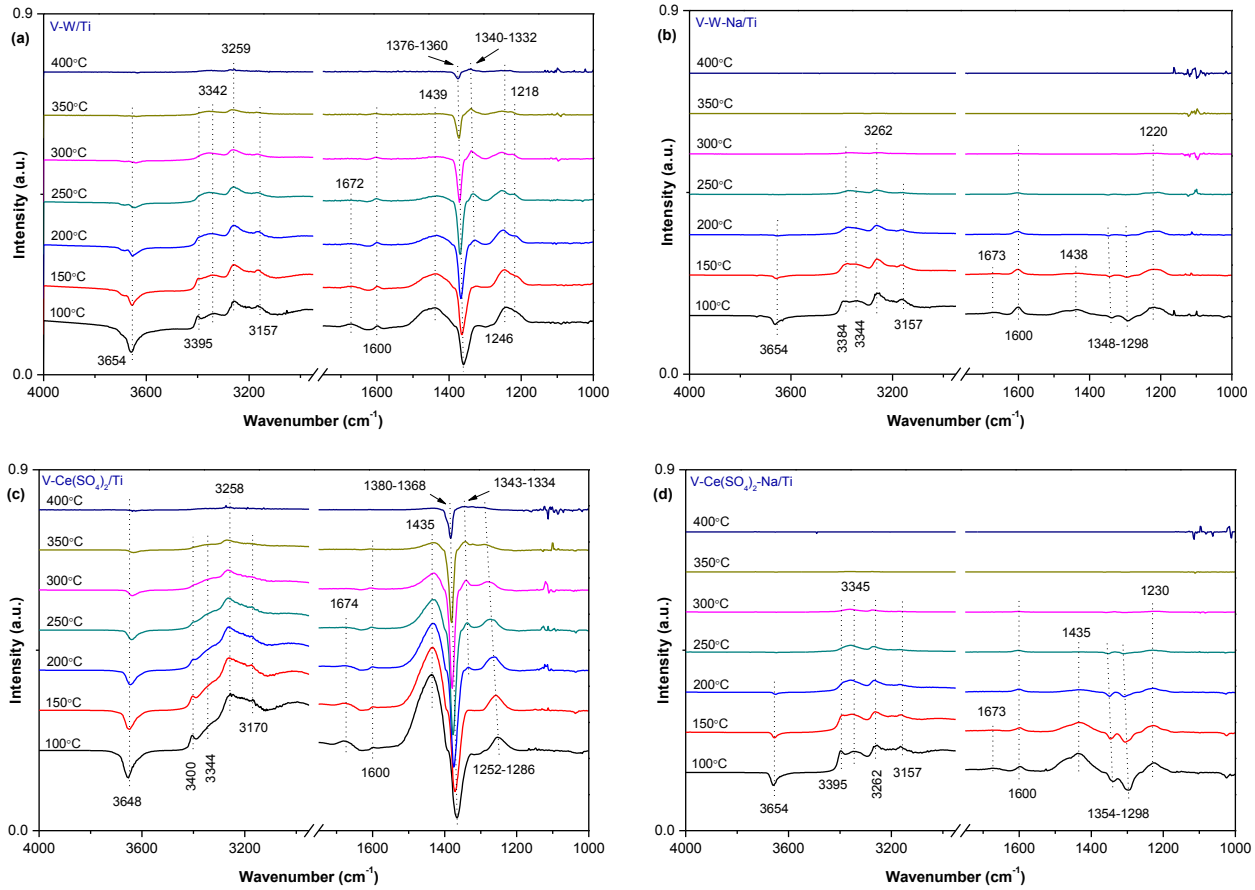

Figure 8. In-situ DRIFTS spectra of NH_3-TPD over the four samples. (a) V-W/Ti, (b) V-W-Na/Ti, (c) V-Ce$(SO_4)_2$/Ti and (d) V-Ce$(SO_4)_2$-Na/Ti.

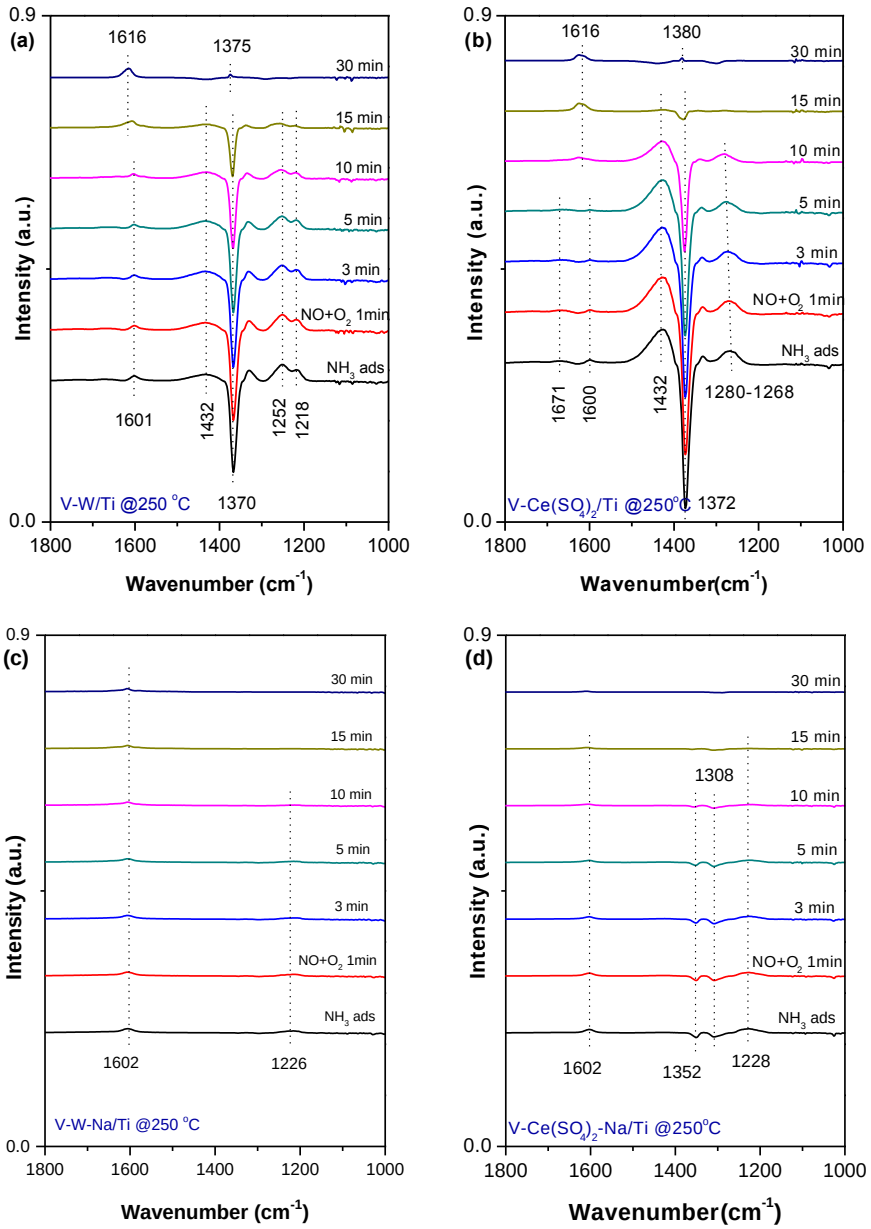

Figure 9. In-situ DRIFTS spectra of reactions between $NO+O_2$ and adsorbed NH_3 species at 250 ˚C over (a) V-W/Ti, (b) V-$Ce(SO_4)_2$/Ti, (c) V-W-Na/Ti, and (d) V-$Ce(SO_4)_2$-Na/Ti.

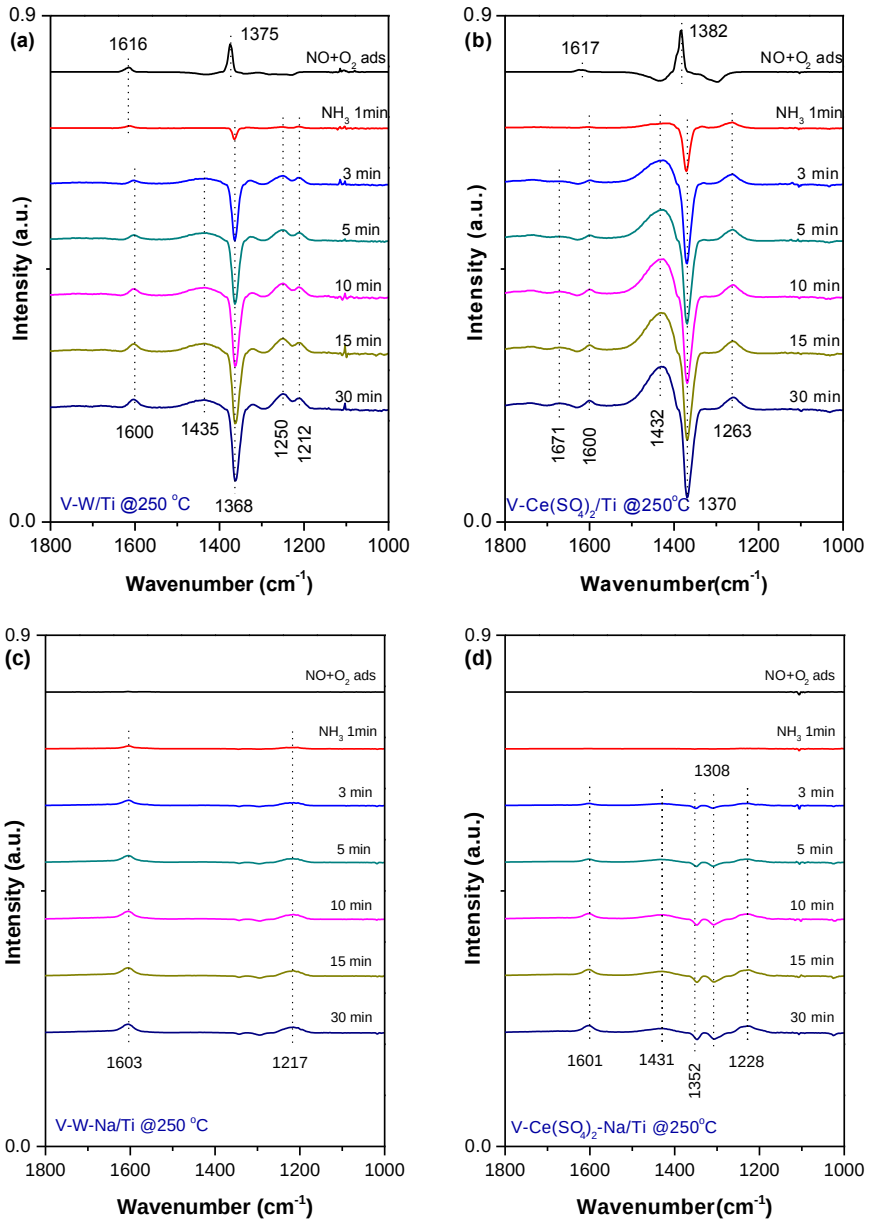

Figure 10. In-situ DRIFTS spectra of reactions between NH_3 and adsorbed $NO+O_2$ species at 250 ˚C over (a) V-W/Ti, (b) V-Ce$(SO_4)_2$/Ti, (c) V-W-Na/Ti, and (d) V-Ce$(SO_4)_2$-Na/Ti.

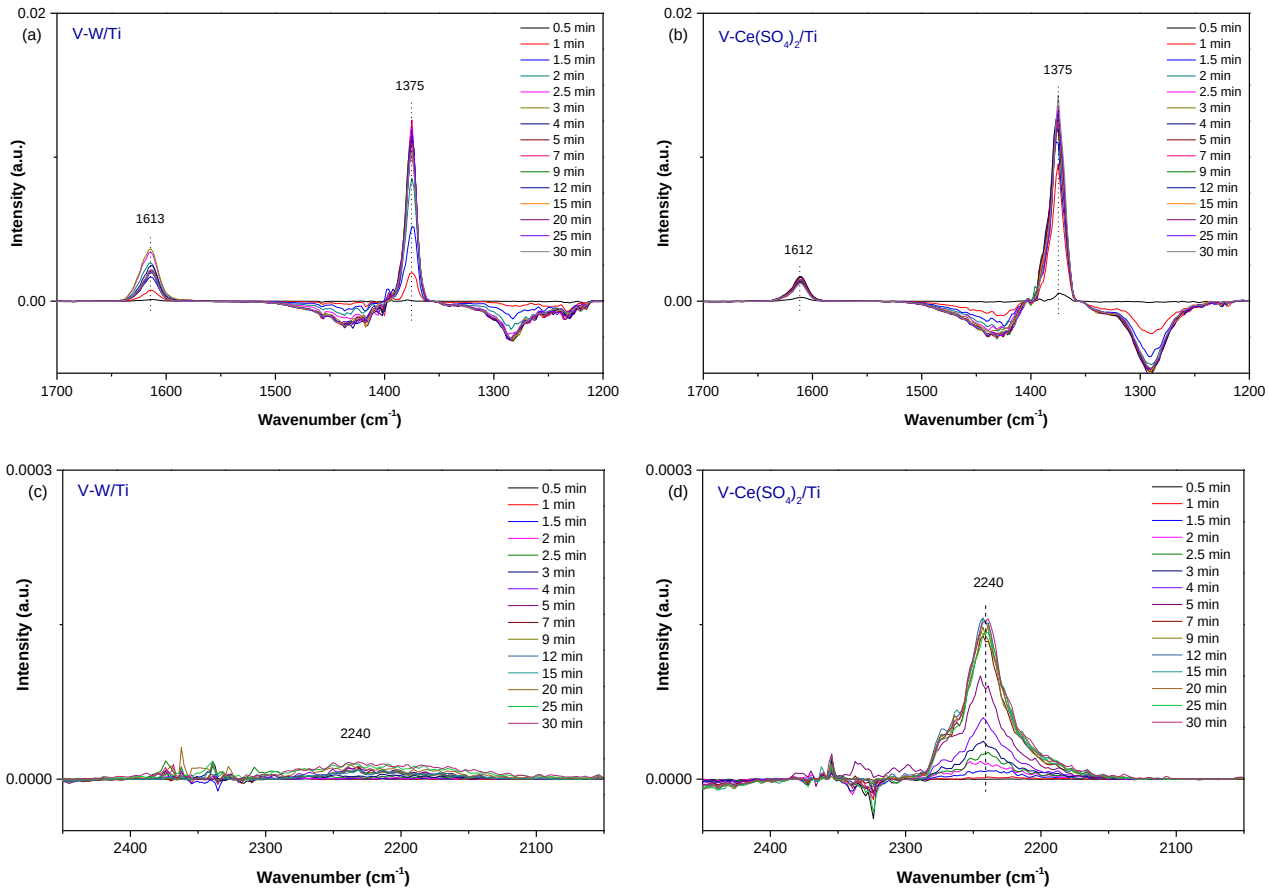

Figure 11. In-situ DRIFTS spectra of transient $NO+O_2$ adsorption over (a) V-W/Ti, range of 1700-1200 cm^{-1}, (b) V-$Ce(SO_4)_2$/Ti, range of 1700-1200 cm^{-1}, (c) V-W/Ti, range of 2450-2050 cm^{-1}, and (d) V-$Ce(SO_4)_2$/Ti, range of 2450-2050 cm^{-1}.

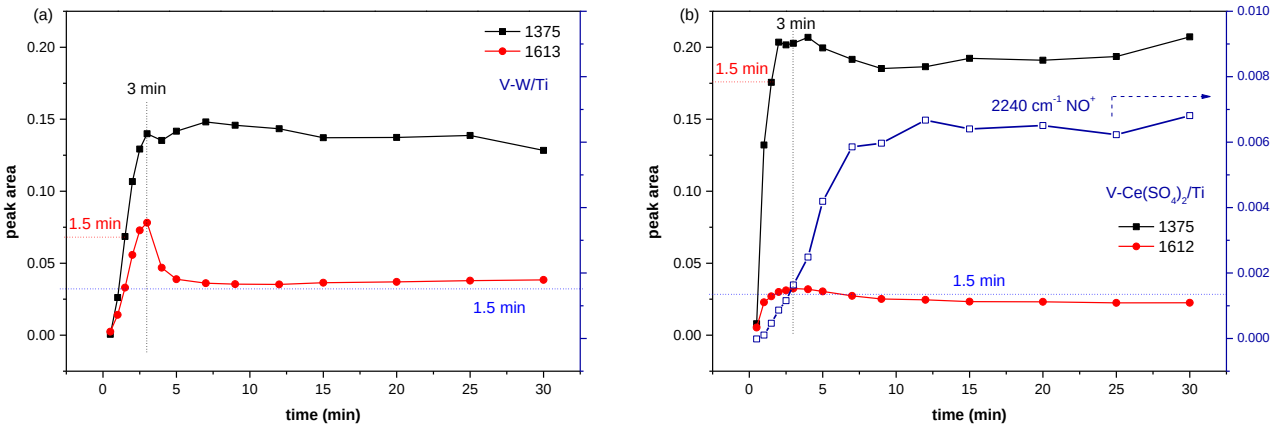

Figure 12. Peak area dynamics of the related in-situ DRIFTS bands during the transient $NO+O_2$ adsorption over (a) V-W/Ti, and (b) V-$Ce(SO_4)_2$/Ti.

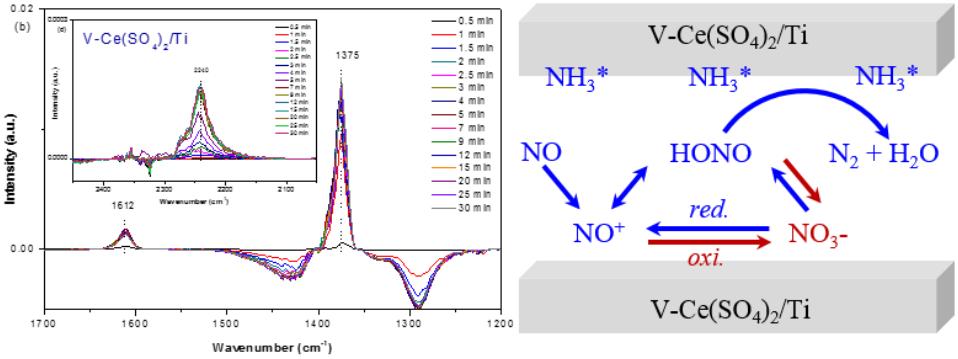
(b)
V-Ce(SO4)2/Ti
1612
1375
0.5 min
1 min
1.5 min
2 min
2.5 min
3 min
4 min
5 min
7 min
9 min
12 min
15 min
20 min
25 min
30 min
Intensity (a.u.)
Wavenumber (cm-1)
V-Ce(SO4)2/Ti
NH3*
NH3*
NH3*
NO
HONO
N2 + H2O
NO+
red.
oxi.
NO3-
V-Ce(SO4)2/Ti